SYNTHESIS OF GOLD NANOPARTICLE CATALYSTS USING A BIPHASIC LIGAND EXCHANGE METHOD AND STUDY OF THEIR ELECTROCATALYTIC PROPERTIES

by

Toma Bhowmick

A Thesis

Submitted to the Faculty of Purdue University

In Partial Fulfillment of the Requirements for the degree of

Master of Science

Department of Chemistry

West Lafayette, Indiana

May 2021

THE PURDUE UNIVERSITY GRADUATE SCHOOL

STATEMENT OF COMMITTEE APPROVAL

Dr. Christina Li, Chair

Department of Chemistry

Dr. Libai Huang

Department of Chemistry

Dr. Corey Thompson

Department of Chemistry

Approved by:

Dr. Christina Hrycena

To my parents, my teachers, and all my family members without whom I won't be here today

ACKNOWLEDGMENTS

First, I would like to thank my advisor, Dr. Christina Li, whom I have admired so much throughout the duration of my time here at Purdue. She has been an excellent mentor in helping me improve on every step, both in research and as a human being. She has been extremely supportive throughout my journey, emotionally as well as a teacher. I will forever be grateful.

Next, I would like to thank my mentor, Vamakshi Yadav. She has been very instrumental in all my research, from helping me collecting data, explaining complicated theories as well as being a mental support during tough times. I will cherish the experience

I would also like to thank my committee members for accepting my request to mentor me. I am very grateful towards them.

Finally, I would like to thank all the Li group members, for making this journey a fun experience. It is very nice to like your colleagues and to be able to be friends with them. They have been extremely helpful and available and I am very thankful for the experience.

Finally, I would like to acknowledge my parents, without whom I would not be here today. All their countless sacrifices made me who I am today, and hopefully in future I can be worthy of all their love and support.

TABLE OF CONTENTS

LIST OF FIGURES

LIST OF TABLES

ABSTRACT

Noble metal nanoparticles have been studied extensively as heterogeneous catalysts for electrocatalytic and thermal reactions. In particular, the support material for the catalytic species is known to play a role in influencing the geometric and electronic properties of the active site as well as its catalytic performance. Polycrystalline gold electrodes have been used as a support to modify the electrocatalytic behavior of adsorbed molecular species. Here, we have studied two electrocatalytic processes- the hydrogen evolution reaction (HER) and the oxygen reduction reaction (ORR), using Au nanoparticle-based catalysts.

Transition metal dichalcogenides are well-known HER catalysts that show structure-sensitive catalytic activity. In particular, undercoordinated sulfur sites at the edges of bulk materials as well as amorphous clusters and oligomers tend to show the highest reactivity. The hydrogen adsorption energy of MoS_x nanoclusters can be further tuned through the metallic support. Here, we synthesize colloidal Au@MoS_4^{2-}, Au@$WS_4^{2-}$and Au@MoS_4^{2-}-WS_4^{2-} using a biphasic ligand-exchange method. The MoS_4^{2-} and WS_4^{2-} complexes show higher HER activity when supported on Au nanoparticles than on to a carbon control, illustrating the electronic role played by the support material.

In the second project, Au nanoparticle cores are utilized as supports for Pd submonolayer and monolayer surfaces in order to catalyze the two-electron reduction of O_2 to generate hydrogen peroxide. Bulk surfaces of Pt and Pd are excellent catalysts for the four-electron reduction of O_2 to H_2O. In order to achieve high selectivity for H_2O_2, we postulate that the ensemble geometry of the Pd surface must be reduced to small islands or single atoms based on literature studies that have shown that large Pd ensembles are required for O–O bond cleavage. In this study, we synthesize several submonolayers surface coverages of Au@Pd core-shell nanoparticles using a biphasic ligand-exchange method. As the Pd coverage decreases from monolayer to submonolayer, the peroxide selectivity rises but is accompanied by an increase in catalytic overpotential. The highest peroxide selectivity was observed for 0.1 layers of Pd on Au, which likely exhibits the highest fraction of isolated atom and small cluster geometric ensembles of Pd.

CHAPTER 1. STUDY OF THE ELECTROCHEMICAL HYDROGEN EVOLUTION REACTION USING COLLOIDAL AU@ MS_4^{2-} (M= Mo, W) CATALYSTS

1.1 Introduction

Achieving efficient hydrogen evolution is critical toward generating renewable H_2 as a fuel for polymer-exchange membrane fuel cells.[1] Molybdenum disulfide and related transition metal dichalcogenide structures are among the most efficient hydrogen evolution reaction (HER) catalysts that do not contain any noble metal components.[2] Metal tetrathiolates and metal disulphides of various structures have been used in synthesizing an array of catalysts in order to replace the traditional noble metal nanoparticle catalysts such as Pt/C.[1-3] Recently, it has been found that $[Mo_3S_{13}]^{2-}$ nanoclusters are highly active for HER and can be further enhanced when supported on metal supports.[4] 2D Metal disulphides have unique structures which have various surface sites that moderate the hydrogen adsorption energy, resulting in a suitable and cheap alternative to the expensive noble metal catalysts.[3-5] In this work, we have supported tetrathiometallate complexes on Au core nanoparticles in order to perturb both its geometric and electronic properties. Biphasic ligand exchange on oleylamine-capped metal nanoparticles have been studied extensive in the semiconductor chemistry where nonpolar ligands are exchanged with polar ligands to give them a charged nature.[6-7] Using this biphasic-ligand exchange method in the synthesis of catalytic nanoparticles is new. It has been observed that supporting the tetrathiolate complexes on nanoparticles induces oligomerization to form an extended two-dimensional structure.[8] At the same time, binding on the nanoparticle surface changes the electronic behavior of the complex, which in turn, alters the surface binding energy of hydrogen atoms, the key intermediate in electrocatalytic HER.[9] Based on these findings, the current study focuses on synthesizing a series of HER catalysts (Au@MoS_4^{2-}, Au@WS_4^{2-} and Au@MoS_4^{2-}-WS_4^{2-}) that show different geometric and electronic properties due to the nature of the ligand-exchange process.

1.2 Materials and method

1.2.1 Material

Gold(III) chloride trihydrate (49.0% Au), ammonium tetrathiomolybdate (99.97%), oleylamine (Oam, technical grade, 70%), molybdenum (IV) sulfide (nanopowder, 90 nm diameter, 99%), Nafion perfluorinated resin solution (5 wt.% in lower aliphatic alcohols and water), and perchloric acid (70%) were purchased from Sigma Aldrich. N-methylformamide (99%) and ammonium tetrathiotungstate (99.9%) were purchased from Alfa Aesar. Hexanes (99.5%), ethanol (99.5%), isopropanol (99.5%), dimethylformamide (99.8%), acetone (99.5%), activated carbon (Darco G-60). All chemicals were used without further purification. Electrolyte solutions were prepared from Nanopure water (ASTM Type I, 18.2 MΩ), purified using a Thermo Scientific Barnstead Ultrapure Water System.

1.2.2 Synthesis of Au nanoparticle

9 nm oleyamine (Oam) capped nanoparticles were synthesized using a previously described procedure.[9] $HAuCl_4 \cdot 3\ H_2O$ (39.4 mg, 0.10 mmol) was dissolved in 10 mL Oam by sonication. The solution was heated in an oil bath at 110 °C with continuous stirring for 40 minutes. Red nanoparticles formed which was cooled at room temperature and precipitated using 20 mL ethanol. The solution was centrifuged for 5 minutes at 8700 rpm, and the supernatant was decanted. The nanoparticles were redissolved in 2 mL toluene, and again precipitated using 40 mL ethanol. This cleaning process was repeated twice. Finally, the particles were dissolved in 10 mL hexanes to prepare a 10 mM stock solution of Au@Oam-capped particles.

1.2.3 Biphasic ligand-exchange of Au@Oam with $(NH_4)_2MoS_4$ and $(NH_4)_2WS_4$

For biphasic exchange of both $(NH_4)_2MoS_4$ and $(NH_4)_2WS_4$, the following procedure was carried out. 1 mL 10 mM (0.01 mmol) Au@Oam solution in hexanes and 1 mL 10 mM (0.1 mmol) $(NH_4)_2MoS_4$ or $(NH_4)_2WS_4$ in DMF were stirred for 10 minutes until the particles went from the hexanes layer to the DMF layer, monitored through the decoloration of the hexanes layer. The upper hexane layer was discarded, and the particles were precipitated using 10 mL acetone. The exchanged particles were redissolved in 1 mL DMF after centrifugation. Finally, the nanoparticles were dissolved in 1 mL DMF, resulting in 10 mM solution of $Au@MoS_4$ or $Au@WS_4$. 1 ml 10

mM Au@Oam solution in hexanes and 0.5 mL 10 mM (0.05 mmol) $(NH_4)_2MoS_4$ and 0.5 mL 10 mM (0.05mmol) $(NH_4)_2WS_4$ in DMF was used simultaneously for the exchange to make Au@MoS_4^{2-}-WS_4^{2-}nanoparticles.

1.2.4 Synthesis of MoS_4^{2-}/C and WS_4^{2-}/C electrochemical controls

6.12 wt% Mo/C control was synthesized by the following procedure. 10 mg $(NH_4)_2MoS_4$ (0.04 mmol) was dissolved in 2 mL nanopure water. 50 mg of activated carbon was added to the solution and strirred for 2 hrs. After that, the mixture was centrifuged, the colorless supernatant was decanted and the solid was dried at room temperature. 6 mg of MoS_4^{2-}/C was mixed in 5 mL of Nafion ink (400 µL Nafion + 2 mL IPA + 7.96 mL H_2O). The mixture was sonicated to prepare catalyst ink for the control sample. In a similar manner, 13 wt.% W/C was synthesized by mixing 6.6 mg of $(NH_4)_2WS_4$ (0.02 mmol) with 50 mg activated carbon Then, 8 mg of WS_4^{2-}/C was sonicated in 5 mL of Nafion solution to prepare the catalyst ink.

1.3 Characterization

1.3.1 Physical Characterization

Transmission electron microscopy (TEM) images were acquired using an FEI Tecnai T20 TEM equipped with a 200 kV LaB_6 filament. Samples for TEM were prepared by drop casting from a 10 mM colloidal solution onto a carbon-coated Cu grid. X-ray fluorescence (XRF) was performed on a Malvern Panalytical Epsilon 4 benchtop energy dispersive XRF spectrometer equipped with an Ag anode X-ray tube.

1.3.2 Electrochemical Characterization

The anodic current is reported as positive and cathodic current as negative. A Ag/AgCl reference (3 M NaCl) electrode was used and the potentials were converted to the real hydrogen electrode (RHE) reference scale using: $E\ (vs\ RHE) = E\ (vs\ Ag/AgCl) + 0.210\ V + 0.0591\ V{*}pH$. The counter electrode used for this experiment was a graphite rod. Hydrogen evolution reactivity (HER) was measured between 0.06 V and –0.33 V vs. RHE for the samples at 20 mV s^{-1} scan rate. The solution was N_2 purged for about 10 minutes prior measurements.

1 µL of each catalyst were drop-casted on small electrode (3 mm), air-dried, and then experiments were carried out.

1.4 Results and discussion

The TEM image in Figure 1.1 shows spherical Au@Oam nanoparticles with sizes ~ 9 nm.

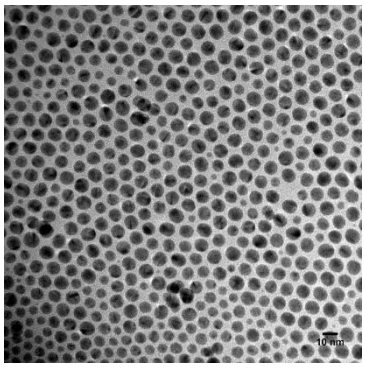

Figure 1.1: TEM image of 9 nm Au@Oam.

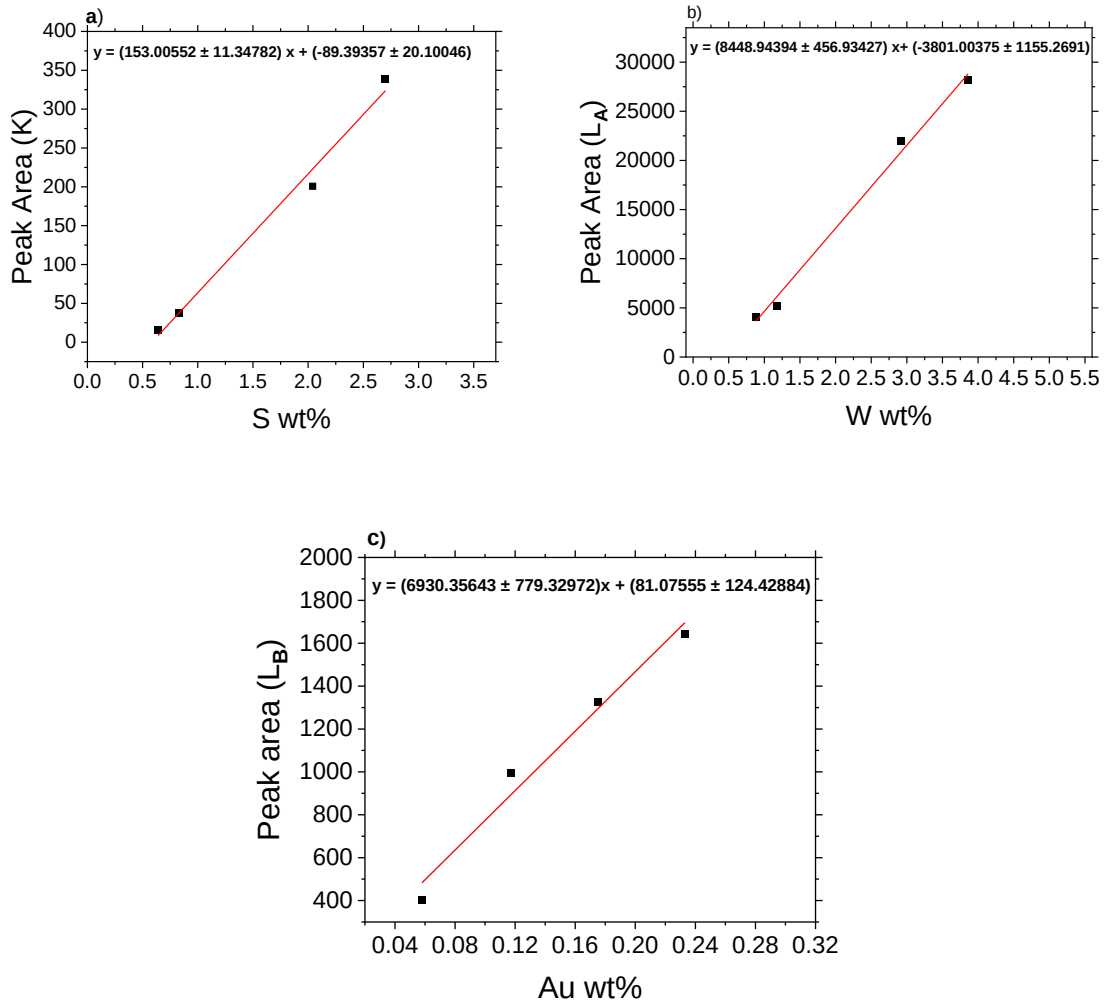

Figure 1.2: XRF Calibration plots for a) S, b) W and c) Au, where K, L_A, and L_B represents respective X-ray absorption edges.

Figure 1.2 shows XRF calibration plots for S, W and Au, respectively where 10 mM Au@Oam was used as the primary source for Au and $(NH_4)_2WS_4$ was used as the source for W and S. The standards peaks were integrated at their respective edges (K edge for S, L_A edge for W and L_B edge for Au). The calibration plots were used to find the atomic percentage of Au to W for 0.01 mmol Au@WS_4^{2-} sample. The atomic ratio was found to be Au:W = 1:1.4.

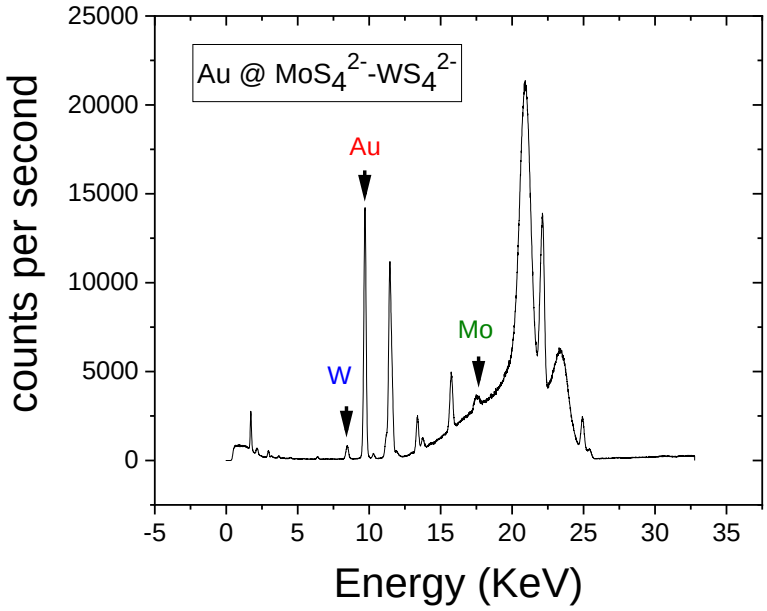

Figure 1.3: XRF spectra of Au@MoS_4^{2-}-WS_4^{2-}.

Figure 1.3 shows the XRF spectra of a 0.01 mmol Au@MoS_4^{2-}-WS_4^{2-} catalyst. The respective W and Mo peaks were too small to integrate, but the amount of both W and Mo on the Au surface are extremely small. It can be concluded from the spectra that the comparatively low Mo and W present on Au surface will have impact on the activity of the catalyst.

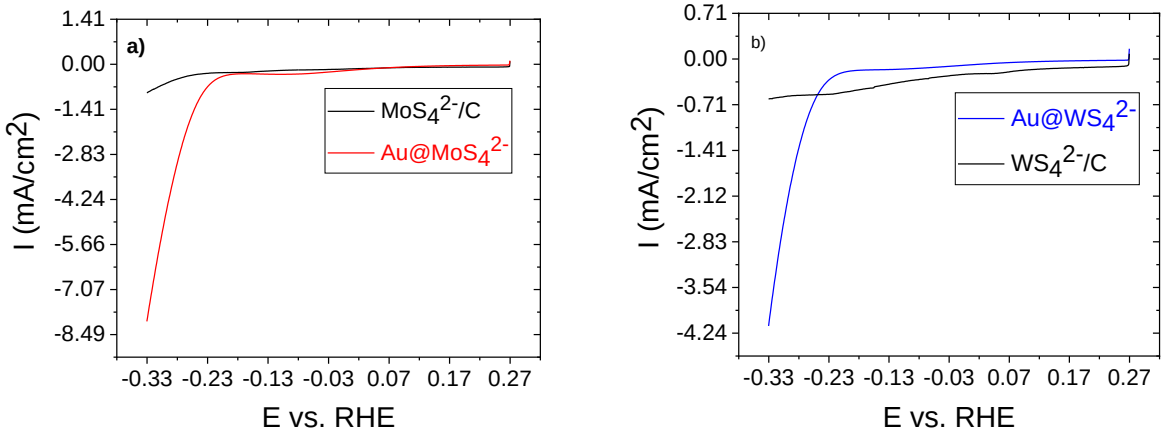

Figure 1.4: HER activity of (a) MoS_4^{2-} /C and Au@MoS_4^{2-} in and (b) WS_4^{2-} /C and Au@ WS_4^{2-} in 1 M $HClO_4$ under N_2 atmosphere.

Figure 1.4 (a) and 1.4 (b) represent HER experiments carried out for $Au@MoS_4^{2-}$ and $Au@WS_4^{2-}$ catalysts under N_2 in 0.1 M $HClO_4$. The current density observed at 0.33 V vs. RHE for $Au@MoS_4^{2-}$ is 8.06 mA/cm^2 and 0.85 mA/cm^2. $Au@WS_4^{2-}$ hits a maximum of 4.17 mA/cm^2 while WS_4^{2-}/C control has a maximum current density of only 0.13 mA/cm^2.

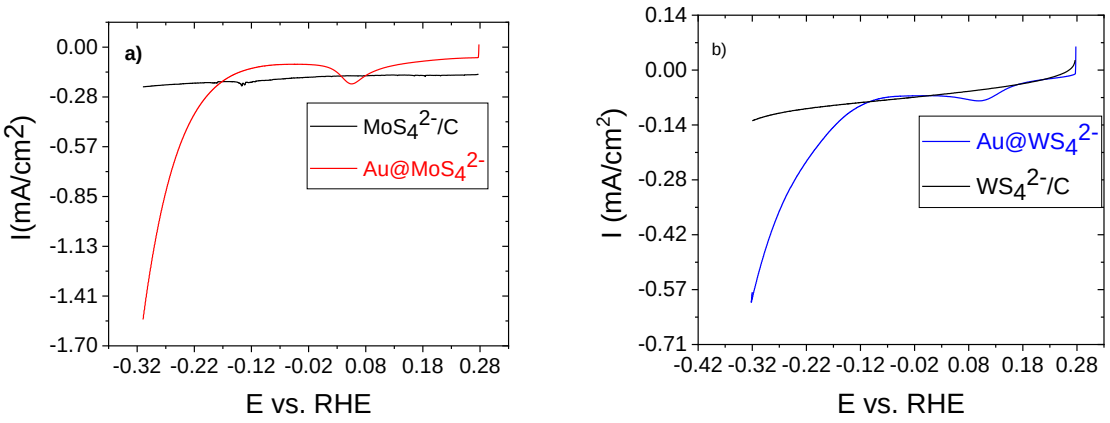

Figure 1.5: HER activity of (a) MoS_4^{2-}/C and $Au@MoS_4^{2-}$ in and (b) WS_4^{2-}/C and $Au@WS_4^{2-}$ in 1 M KOH under N_2 atmosphere.

Figure1.5 (a) and 1.5 (b) represent experiments HER carried out for $Au@MoS_4^{2-}$ and $Au@WS_4^{2-}$ catalysts under N_2 in 0.1 M KOH. The current density observed at 0.33 V vs. RHE for $Au@MoS_4^{2-}$ is 1.56 mA/cm^2 and 0.26 mA/cm^2.for MoS_4^{2-}/C. $Au@WS_4^{2-}$ hits a maximum of 0.63 mA/cm^2 while WS_4^{2-}/C control sample has a maximum current density of 0.14 mA/cm^2.

In both acidic and alkaline electrolytes, the $Au@MoS_4^{2-}$ and $Au@WS_4^{2-}$ catalysts show much higher HER current than the MoS_4^{2-} and WS_4^{2-} on carbon controls. This indicates that there is some electronic and geometric modification of the tetrathiometallate complex due to the Au surface, which results in higher catalytic performance. In comparison with the alkaline condition, acidic electrolyte shows have better performance for HER catalysis in both cases. This can be because the catalyst becomes unstable in basic condition and starts to dissolve away from the electrode. In comparing comparing MoS_4^{2-} to WS_4^{2-} under similar conditions (1 µL of 10 mM catalyst), $Au@MoS_4^{2-}$ has higher HER current density than $Au@WS_4^{2-}$ at 0.33 V vs. RHE. Since further characterization was not carried out, it is hard to talk about absolute activity of the two catalysts. In part, fewer surface W atoms supported on Au relative to Mo due to the bulkier size of WS_4^{2-} may contribute to the lower activity. Electronically, we anticipate that the W-S bonds are

stronger than Mo-S bonds, which would result in weaker hydride adsorption and and faster HER turnover on the $Au@WS_4^2$ sulphur sites. As a result, we believe that the number no. of available ligands on the Au surface may be playing an important role. Moreover, under HER catalytic conditions, the tetrathiometallate ligands tend to oligomerize and form different geometric structures, which may also be responsible for the variation in activity observed between $Au@MoS_4^{2-}$ and $Au@WS_4^{2-}$.[9]

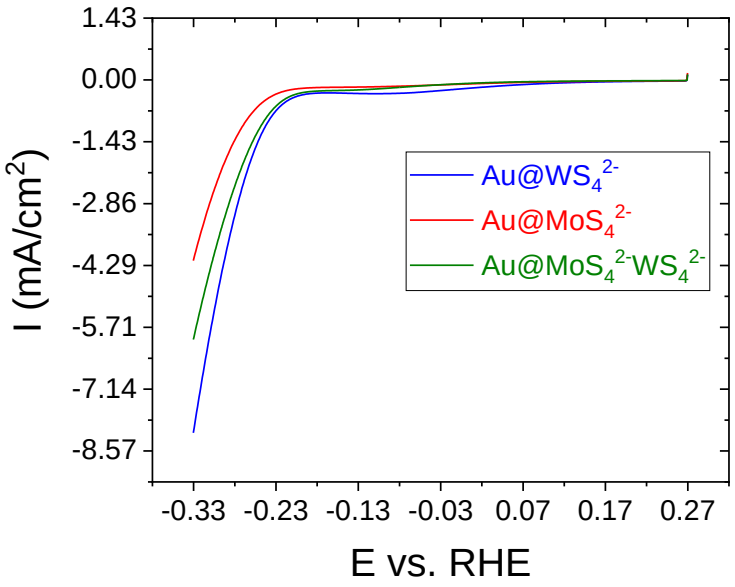

Figure 1.6: HER activity $Au@MoS_4^{2-}$- WS_4^{2-} in 1 M $HClO_4$ under N_2 atmosphere.

From Figure 1.6, at –0.33 V vs. RHE in 1 M $HClO_4$ the activity of $Au@MoS_4^{2-}$-WS_4^{2-} falls in between the catalytic activity of $Au@MoS_4^{2-}$ and $Au@WS_4^{2-}$, giving a geometric current of 6.14 mA/cm^2. This arises from the fact that a mixture of MoS_4^{2-} and $WS_4^{2-}$are adsorbed on the surface of Au and appear to act relatively independently of each other in terms of their HER catalysis.

1.5 Conclusion

In conclusion, a biphasic-ligand exchange method could be used to synthesize MoS_4^{2-} and WS_4^{2-}-capped Au nanoparticles by replacing oleylamine from Au@Oam. The exchanged particles could be used as catalysts in the hydrogen evolution reaction in both acidic and alkaline media.

Both $Au@MoS_4^{2-}$ and $Au@WS_4^{2-}$ showed better catalytic performance than the bare tetrathiolates adsorbed on carbon. The enhancement of performance was due to both the electronic and the geometric effect exerted on the surface-bound tetrathiolate ligands, which moderates their hydrogen adsorption energy and therefore impacts their HER catalytic activity. Furthermore, it was observed that $Au@MoS_4^{2-}$ had better catalytic activity than $Au@WS_4^{2-}$, which could be due to the number of active surface bound Mo being greater than W, affecting the available active sites for catalysis. The $Au@MoS_4^{2-}$-WS_4^{2-} activity fell in between the pure $Au@WS_4^{2-}$ and $Au@MoS_4^{2-}$ catalysts, suggesting that no significant interaction between the surface tetrathiometallates takes place.

1.6 References

(1) Benck, J. D.; Hellstern, T. R.; Kibsgaard, J.; Chakthranont, P.; Jaramillo, T. F. Catalyzing the Hydrogen Evolution Reaction (HER) with Molybdenum Sulfide Nanomaterials. *ACS Catalysis*. American Chemical Society October 8, 2014, pp 3957–3971. https://doi.org/10.1021/cs500923c.

(2) Chatterjee, S.; Sengupta, K.; Dey, S.; Dey, A. Ammonium Tetrathiomolybdate: A Versatile Catalyst for Hydrogen Evolution Reaction from Water under Ambient and Hostile Conditions. *Inorg. Chem.* **2013**, *52* (24), 14168–14177. https://doi.org/10.1021/ic402056k.

(3) Cheng, L.; Huang, W.; Gong, Q.; Liu, C.; Liu, Z.; Li, Y.; Dai, H. Ultrathin WS_2 Nanoflakes as a High-Performance Electrocatalyst for the Hydrogen Evolution Reaction. *Angew. Chemie Int. Ed.* **2014**, *53* (30), 7860–7863. https://doi.org/10.1002/anie.201402315.

(4) Hellstern, T. R.; Kibsgaard, J.; Tsai, C.; Palm, D. W.; King, L. A.; Abild-Pedersen, F.; Jaramillo, T. F. Investigating Catalyst-Support Interactions to Improve the Hydrogen Evolution Reaction Activity of Thiomolybdate $[Mo_3S_{13}]^{2-}$ Nanoclusters. *ACS Catal.* **2017**, *7* (10), 7126–7130. https://doi.org/10.1021/acscatal.7b02133.

(5) Li, Y.; Wang, H.; Xie, L.; Liang, Y.; Hong, G.; Dai, H. MoS_2 Nanoparticles Grown on Graphene: An Advanced Catalyst for the Hydrogen Evolution Reaction. *J. Am. Chem. Soc.* **2011**, *133* (19), 7296–7299. https://doi.org/10.1021/ja201269b.

(6) Fafarman, A. T.; Koh, W. K.; Diroll, B. T.; Kim, D. K.; Ko, D. K.; Oh, S. J.; Ye, X.; Doan-Nguyen, V.; Crump, M. R.; Reifsnyder, D. C.; Murray, C. B.; Kagan, C. R. Thiocyanate-Capped Nanocrystal Colloids: Vibrational Reporter of Surface Chemistry and Solution-Based Route to Enhanced Coupling in Nanocrystal Solids. *J. Am. Chem. Soc.* **2011**, *133* (39), 15753–15761. https://doi.org/10.1021/ja206303g.

(7) Choi, J.-H.; Soong; Oh, J.; Lai, Y.; Kim, D. K.; Zhao, T.; Fafarman, A. T.; Diroll, B. T.; Murray, C. B.; Kagan, C. R. In Situ Repair of High-Performance, Flexible Nanocrystal Electronics for Large-Area Fabrication and Operation in Air. https://doi.org/10.1021/nn403752d.

(8) Yadav, V.; Lowe, J. S.; Shumski, A. J.; Liu, E. Z.; Greeley, J.; Li, C. W. Modulating the Structure and Hydrogen Evolution Reactivity of Metal Chalcogenide Complexes through Ligand Exchange onto Colloidal Au Nanoparticles. *ACS Catal.* **2020**, *10* (22), 13305–13313. https://doi.org/10.1021/acscatal.0c02895.

(9) Huang, X.; Shumski, A. J.; Zhang, X.; Li, C. W. Systematic Control of Redox Properties and Oxygen Reduction Reactivity through Colloidal Ligand-Exchange Deposition of Pd on Au. *J. Am. Chem. Soc.* **2018**, *140* (28), 8918–8923. https://doi.org/10.1021/jacs.8b04967.

CHAPTER 2. STUDY OF THE ELECTROCHEMICAL OXYGEN REDUCTION REACTION USING COLLOIDAL GOLD-PALLADIUM CATALYST

2.1 Introduction

Noble metal catalysts like Pd and Pt have been very instrumental in alkaline oxygen reduction reaction.[1] Due to their surface electronic properties, these catalysts show great performance in the preferential four electron reduction of oxygen, i.e., production of water.[2] But to tune these catalyts towards the production of hydrogen peroxide, catalysts must go through a two electron reduction step, which is difficult to achieve in a selective fashion.[3] Various geometries of Pt and Pd metal catalysts such as nanorods and nanosheets have been studied in order to enhance the ORR catalytic activity.[4-5] Strain effects in core-shell nanoparticles have also been found to enhance the performance of monolayer Pt catalyst ($Pt/Co_5/C$).[6] In recent work, it has been found that supporting palladate ions onto a noble metal surface, Au, can tune both ensemble geometry and electronic properties.[7] A range of gold Au@Pd core-shell nanoparticles ranging from sub-monolayer to multilayer was synthesized and a peroxide selectivity of 60% was achieved for the 0.3 layer (L) sample.[8] As the surface Pd coverage was increased from submonolayer to a complete shell, the four electron reduction of O_2 became more favorable. It was also found that as the layer thickness varied, the PdO reduction peak in cyclic voltammetry shifted positively by over 240 mV. Based on these findings, the current study focuses on using these submonolayer core-shell materials in acidic ORR to understand the role of ensemble geometry and electronic properties indicating the selectivity toward hydrogen peroxide production. We hypothesize that low submonolayer coverages of Pd on Au will reduce the Pd catalytic ensemble such that O–O bond cleavage is disfavored, and hydrogen peroxide is preferentially produced as the O_2 reduction product

2.2 Materials and method

2.2.1 Materials

Gold(III) chloride trihydrate (49.0% Au), oleylamine (Oam, technical grade, 70%), tetrabutylammonium chloride hydrate (98%), and perchloric acid (70%) were purchased from

Sigma Aldrich. N-methylformamide (99%) was purchased from Alfa Aesar. Potassium tetrachloropalladate(II) (32.0% Pd) was purchased from Acros Organics. Toluene (99.5%), ethanol (99.5%), methanol (99.9%), isopropanol (99.5%), and dimethylformamide (99.8%), acetone (99.5%) were purchased from Fisher Scientific. Oxygen (99.99%) and nitrogen (99.99%) were purchased from Indiana Oxygen. All chemicals were used without further purification. Electrolyte solutions were prepared from Nanopure water (ASTM Type I, 18.2 MΩ), purified using a Thermo Scientific Barnstead Ultrapure Water System.

2.2.2 Synthesis of Au nanoparticle

9 nm oleyamine (Oam) capped nanoparticles were synthesized using a previously described procedure.[8] $HAuCl_4 \cdot 3\ H_2O$ (39.4 mg, 0.10 mmol) was dissolved in 10 mL OAm by sonication. The solution was heated in an oil bath at 110 °C with continuous stirring for 40 minutes. Red nanoparticles formed which was cooled at room temperature and precipitated using 40 mL ethanol. The solution was centrifuged for 5 minutes at 8700 rpm, and the supernatant was decanted. The nanoparticles were redissolved in 2 mL toluene, and again precipitated using 20 mL ethanol. This cleaning process was repeated twice. Finally, the particles were dissolved in 10 mL hexanes to prepare a 10 mM stock solution of Au@Oam-capped particles.

2.2.3 Biphasic ligand exchange using K_2PdCl_4 ligand

For biphasic exchange of both $(NH_4)_2MoS_4$ and $(NH_4)_2WS_4$, the following procedure was carried out.[8] Fresh stock solutions of K_2PdCl_4 (10 mM) in NMF, NBu_4Cl (1 M or 0.1 M) in DMF were prepared before each ligand-exchange reaction, and all reagents were taken from these stock solutions. K_2PdCl_4 (5 μmol) and NBu_4Cl (5 μmol) were diluted into 2 mL of a 1:1 NMF:H_2O solvent mixture (polar). Separately, colloidal Au@OAm NPs (10 μmol by Au atom%) were diluted into 6 mL of toluene (nonpolar). The nonpolar solution was layered on top of the polar solution in a 50 mL centrifuge tube and stirred vigorously until the nonpolar layer became clear and a purple suspension formed at the interface and in the polar layer. At this ratio of NBu_4Cl:K_2PdCl_4 (1:1), the exchange reaches completion in 9-12 hours. For a 10:1 and 100:1 ratio of NBu_4Cl:K_2PdCl_4, the exchange takes 3-5 and 1-2 hours, respectively. The biphasic solution was centrifuged at 8500 rpm for 5 min. and the nonpolar layer was removed by pipet. The nanoparticles were precipitated

using 2.5 mL of acetone, centrifuged, and collected after decanting the liquid. The exchanged nanoparticles were redissolved in 1 mL DMF to form a dark red-purple solution with nominal concentration of 10 mM based on Au atom%. To vary the coverage of $PdCl_4^{2-}$ on Au after the exchange, the ratio of NBu_4Cl:K_2PdCl_4 in the polar layer was varied as indicated in Table 1.

Table 1:.Equivalents of NBu_4Cl and K_2PdCl_4 required to synthesize each Au@Pd layer

Sample	Pd (eq. wrt Au)	NBu_4Cl (eq. wrt Au)
0.1L	0.5	50
0.4L	0.5	18
0.9L	0.5	0.5

2.3 Characterization

2.3.1 Electrochemical methods

A Pine Wave Driver 20 Bipotentiostat was used for all experiments. The working electrode was prepared by drop-drying 5 μL of a 10 mM colloidal nanoparticle solution in DMF onto a polished glassy carbon electrode with 5 mm diameter (Pine). The counter electrode was a graphite rod. The electrolyte used for ORR electrochemical experiments was 0.1 M $HClO_4$ with pH of 1 and 0.1 M KOH with pH of 13 for cyclic voltammetry. Currents are reported with anodic current as positive and cathodic current as negative. Potentials were measured against a Hg/HgO reference (0.1 M KOH, Pine) and a Ag/AgCl reference (3 M NaCl) electrode (0.1 M $HClO_4$, Pine) and converted to the RHE reference scale using E (vs RHE) = E (vs Hg/HgO) + 0.165V + 0.0591 V*pH and E (vs RHE) = E (vs Ag/AgCl) + 0.21V + 0.0591 V*pH.

Oxygen reduction reaction (ORR) voltammetry was carried out using a rotating ring-disk electrode in a single-compartment glass cell (Pine). The solution was purged with O_2 for at least 30 min prior to the start of the experiment. For all ORR experiments, a rotation rate of 1600 rpm and scan rate of 20 mV/s were utilized. Five cyclic voltammetry (CV) scans were collected prior to running a linear sweep voltammetry (LSV) scan, with the ring held at 500 mV vs Hg/HgO. LSV data was collected by sweeping from positive to negative potential because this scan direction most resembled steady state behavior.

From the ring current, the peroxide selectivity is calculated based on the following equations:

$\% H_2O_2 = (2I_R / N) / (I_R/N) + I_D$

where I_R = ring current

I_D = disk current

N = 0.247, the collection efficiency of the Pt ring

2.4 Results and discussion

Figure 2.1 shows the cyclic voltammetry features of 0.3 L and 0.9 L Au@Pd surfaces where the Pd oxidation peak shows up around 0.84 V vs RHE and the Au oxidation peak is observed at 1.12 V vs. RHE.

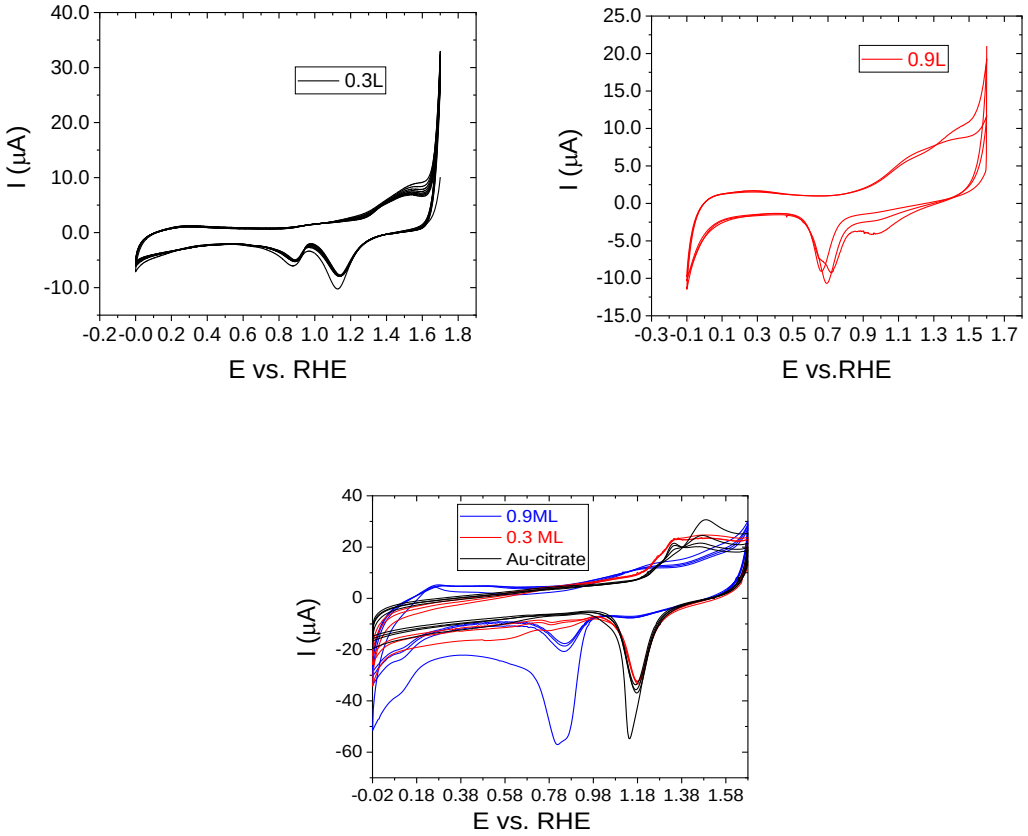

Figure 2.1: Cyclic voltammetry of 0.3 L and 0.9 L coverage Au@Pd samples.

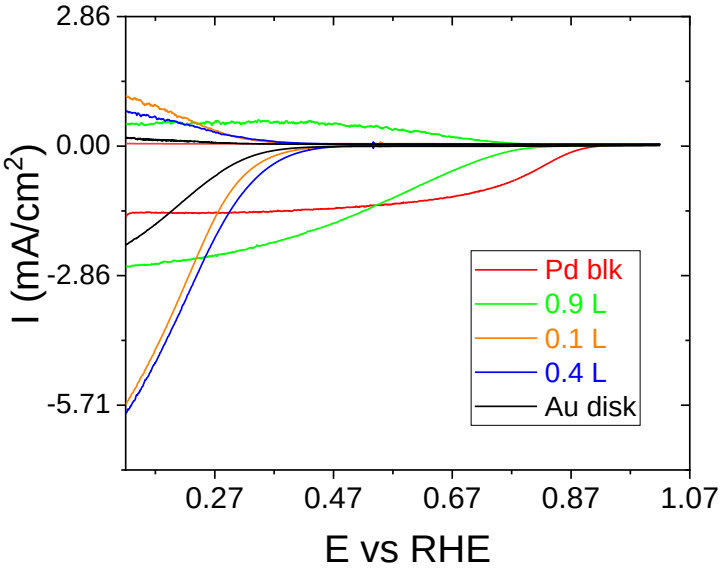

Figure 2.2: ORR activity of different catalyst coverages.

Figure 2.2 shows the ORR disk and ring current densities for several submonolayer Au@Pd catalysts. At 0.1 L Au@Pd, the onset potential for ORR is 0.33 V vs. RHE and the current density reaches 2.17 mA/cm^2 at the most negative point in the linear sweep voltammogram. As we increase the Pd coverage to 0.9 L, we observe that the onset potential shifts positively by 0.34 V to 0.67 V vs. RHE. The limiting current density now reaches 4.45 mA/cm^2, much closer to the expected mass-transport limit in $HClO_4$ electrolyte. Compared to Pd black, however, the 0.9 L Au@Pd catalyst still shows much higher overpotential for ORR. Pd black onsets at 0.84 V vs. RHE and reaches a limiting current density of 5.21 mA/cm^2. To better understand the trends as a function of Pd coverage in Au@Pd core-shell nanoparticles, we have extracted several key metrics for the ORR activity and selectivity including the disk current half-wave potential ($E_{1/2}$), disk current onset potential (E_{onset}), maximum ring current density (j_R max), and hydrogen peroxide selectivity.

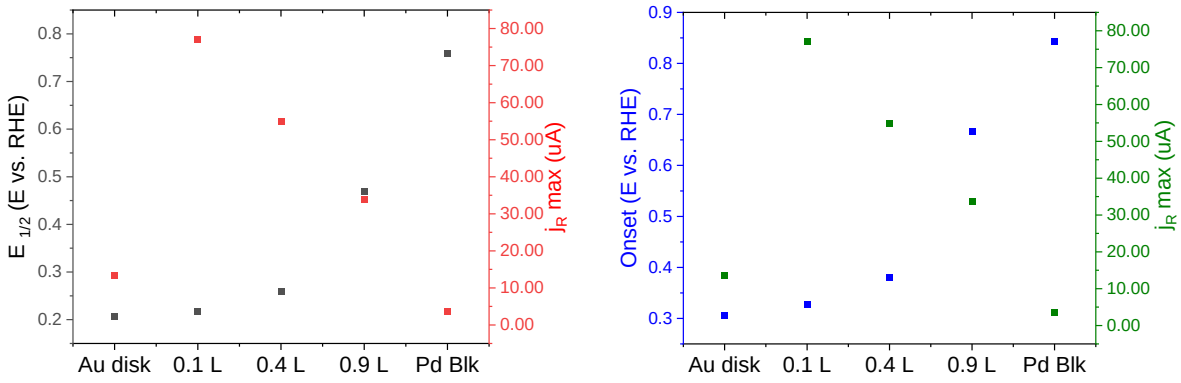

Figure 2.3: Comparison plot for $E_{1/2}$ and maximum ring current of catalyst samples.

Figure 2.3 (left) plots both $E_{1/2}$ and maximum ring current density (j_R) for the pure Au and pure Pd controls as well as varying Au@Pd coverages. The pure Au disk has the most negative $E_{1/2}$ value of the samples studied at 0.21 V vs. RHE. As we add Pd to the surface of Au, we find that $E_{1/2}$ increases from 0.22 V to 0.47 V from 0.1 L to 0.9 L Au@Pd. Finally, the Pd black catalyst shows the highest $E_{1/2}$ potential of 0.76 V vs. RHE. Interestingly, the maximum ring current density shows an inverted relationship to Pd coverage on Au. For the Au disk, j_R is observed to be 13.5 µA. At the lowest coverage of Pd on Au (0.1 L), we observe a large jump in ring current density to 77 µA. As we increased the Pd coverage from 0.1 L to 0.9 L, we observe a gradual decrease in j_R current. At , 0.4 L and 0.9 L Au@Pd, 55 µA and 33.8 µA of ring current are observed, respectively. Finally, for Pd black, we observe the lowest ring current of 3.5 µA. These data clearly show that low coverages of Pd on Au are indeed more capable of generating the two-electron product, hydrogen peroxide, compared to large ensembles and pure Pd surfaces. Figure 2.4 (right) plots the E_{onset} and maximum ring current density (j_R) for the same samples. The trend in onset potential is essentially identical to that observed for $E_{1/2}$. From the bare Au surface to submonolayer Au@Pd coverages, the onset potential for the disk current continually increases from 0.31 V to 0.67 V vs. RHE. Pd black had the most positive onset potential value of 0.84 V vs. RHE.

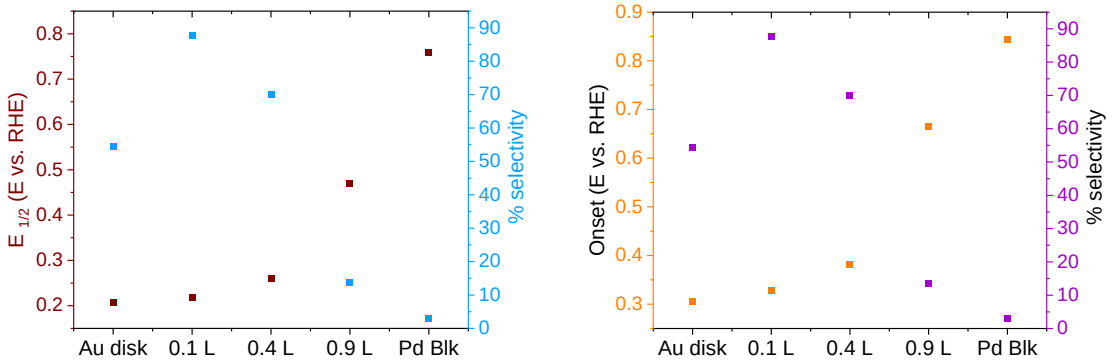

Figure 2.4: Comparison plot for $E_{1/2}$ and maximum ring current of catalyst samples.

Next, we utilized the ring and disk current densities observed above to calculate the peroxide selectivity for each sample. Figure 2.4 plots $E_{1/2}$ (left) and E_{onset} (right) along with peroxide selectivity for all samples studied. The peroxide selectivity on a pure Au disk catalyst was reasonably high at 54 %. For the 0.1 L Au@Pd coverage, we observed a peak peroxide selectivity of 88%. As we increased the coverage of Pd from 0.1 L to 0.9 L, the selectivity decreased to 71% and 14 % at 0.4 L and 0.9 L, respectively. Pd black exhibited extremely low peroxide selectivity at 3 %. These data support our hypothesis that ensemble geometry plays a critical role in dictating ORR selectivity to hydrogen peroxide. At the lowest Pd coverage, the Pd ensembles are sufficiently small that cleavage of the O–O bond in O_2 is disfavored and hydrogen peroxide is preferentially released. While the exposed Au surface certainly plays some role in this high peroxide selectivity, the maximum ring current densities for pure Au compared to 0.1 L Au@Pd suggest that the majority of the peroxide current density stems from the surface Pd layer. As the Pd ensemble size increases in the near monolayer Au@Pd sample, the peroxide selectivity drops precipitously while the $E_{1/2}$ and E_{onset} are still strongly perturbed relative to the pure Pd control. These data suggest that the 0.9 L Au@Pd primarily experiences an electronic perturbation due to the Au core but no ensemble geometry change. Based on these data, we now have a system that allows us to continuously tune both the redox properties and ensemble geometry of Pd catalytic active sites. The optimal catalysts for high reactivity and selectivity toward O_2 reduction to hydrogen peroxide are submonolayer Au@Pd structures ranging in coverage from 0.1 to 0.4 L of Pd on Au.

2.5 Conclusion

In this study, we synthesized various surface coverages of Au@Pd catalyst and analyzed their catalytic activity towards the oxygen reduction reaction. For 0.1 L Au@Pd, we observed the highest ring current of 77 μA and peroxide selectivity of 88 %. As we increased the Pd coverage, the ring current and peroxide selectivity decreased significantly with 0.9 L Au@Pd having only 14 % peroxide selectivity. This data support our hypothesis that ensemble geometry plays a critical role in dictating the selectivity of Pd-catalyzed ORR reactivity in acidic media.

2.6 References

(1) Benck, J. D.; Hellstern, T. R.; Kibsgaard, J.; Chakthranont, P.; Jaramillo, T. F. Catalyzing the Hydrogen Evolution Reaction (HER) with Molybdenum Sulfide Nanomaterials. *ACS Catalysis*. American Chemical Society October 8, 2014, pp 3957–3971. https://doi.org/10.1021/cs500923c.

(2) Chen, C.; Xing, G.; Wang, J.; Zhao, Y.; Li, B.; Tang, J.; Jia, G.; Wang, T.; Sun, J.; Xing, L.; Yuan, H.; Gao, Y.; Meng, H.; Chen, Z.; Zhao, F.; Chai, Z.; Fang, X. Multihydroxylated $[Gd@C_{82}(OH)_{22}]_n$ Nanoparticles: Antineoplastic Activity of High Efficiency and Low Toxicity. *Nano Lett.* **2005**, *5* (10), 2050–2057. https://doi.org/10.1021/nl051624b.

(3) Shao, M.; Yu, T.; Odell, J. H.; Jin, M.; Xia, Y. Structural Dependence of Oxygen Reduction Reaction on Palladium Nanocrystals. *Chem. Commun.* **2011**, *47* (23), 6566–6568. https://doi.org/10.1039/c1cc11004g.

(4) Xiao, L.; Zhuang, L.; Liu, Y.; Lu, J.; Abruña, H. D. Activating Pd by Morphology Tailoring for Oxygen Reduction. *Journal of the American Chemical Society*. American Chemical Society January 21, 2009, pp 602–608. https://doi.org/10.1021/ja8063765.

(5) Lu, Y.; Jiang, Y.; Gao, X.; Wang, X.; Chen, W. Strongly Coupled Pd Nanotetrahedron/Tungsten Oxide Nanosheet Hybrids with Enhanced Catalytic Activity and Stability as Oxygen Reduction Electrocatalysts. *J. Am. Chem. Soc.* **2014**, *136* (33), 11687–11697. https://doi.org/10.1021/ja5041094.

(6) Lima, F. H. B.; Zhang, J.; Shao, M. H.; Sasaki, K.; Vukmirovic, M. B.; Ticianelli, E. A.; Adzic, R. R. Catalytic Activity - d-Band Center Correlation for the O_2 Reduction Reaction on Platinum in Alkaline Solutions. *J. Phys. Chem. C* **2007**, *111* (1), 404–410. https://doi.org/10.1021/jp065181r.

(7) Zhang, K.; Hu, X.; Liu, J.; Yin, J. J.; Hou, S.; Wen, T.; He, W.; Ji, Y.; Guo, Y.; Wang, Q.; Wu, X. Formation of PdPt Alloy Nanodots on Gold Nanorods: Tuning Oxidase-like Activities via Composition. *Langmuir* **2011**, *27* (6), 2796–2803. https://doi.org/10.1021/la104566e.

(8) Huang, X.; Shumski, A. J.; Zhang, X.; Li, C. W. Systematic Control of Redox Properties and Oxygen Reduction Reactivity through Colloidal Ligand-Exchange Deposition of Pd on Au. *J. Am. Chem. Soc.* **2018**, *140* (28), 8918–8923. https://doi.org/10.1021/jacs.8b04967.